

UC Irvine

UC Irvine Previously Published Works

Title

Multicolor Photonic Pigments for Rotation-Asymmetric Mechanochromic Devices

Permalink

<https://escholarship.org/uc/item/06h5113c>

Journal

Advanced Materials, 34(4)

ISSN

0935-9648

Authors

Li, Zhiwei

Wang, Xiaojing

Han, Lili

et al.

Publication Date

2022

DOI

10.1002/adma.202107398

Copyright Information

This work is made available under the terms of a Creative Commons Attribution-NonCommercial License, available at <https://creativecommons.org/licenses/by-nc/4.0/>

Peer reviewed

# Multicolor photonic pigments for rotation-asymmetric mechanochromic devices

Zhiwei Li, Xiaojing Wang, Lili Han, Chenhui Zhu, Huolin Xin, and Yadong Yin

Dr. Z. Li, Dr. X. Wang, Prof. Y. Yin

Department of Chemistry, University of California, Riverside, California 92521, United States

Email: [yadong.yin@ucr.edu](mailto:yadong.yin@ucr.edu)

Dr. L. Han, Prof. H. L. Xin

Department of Physics and Astronomy, University of California-Irvine, Irvine, California 92697, United States

Prof. C. Zhu

Advanced Light Source, Lawrence Berkeley National Laboratory, Berkeley, California 94720, USA

Keywords: photonic crystals, photonic pigments, structural colors, magnetic assembly, mechanochromic devices, orientational control

**Abstract:** Photonic crystals have been extensively explored to replace inorganic pigments and organic dyes as coloring elements in printing, painting, sensing, and anti-counterfeiting due to their brilliant structural colors, chemical stability, and environmental friendliness. However, most existing photonic-crystal-based pigments can only display monochromatic colors once made, and generating multicolors has to start with designing different building blocks. Here, we report a novel photonic pigment featuring highly tunable structural colors in the entire visible spectrum, made by the magnetic assembly of monodisperse nanorods into body-centered tetragonal photonic crystals. Their prominent magnetic and crystal anisotropy makes it efficient to generate multicolors using one photonic pigment by magnetically controlling the crystal orientation. Further, the combination of angle-dependent diffraction and magnetic orientation control enables the design of rotation-asymmetric photonic films that display distinct patterns and encrypted information in response to rotation. The efficient multicolor generation through precise orientational control makes this novel photonic pigment promising in developing high-performance structural colored materials and optical devices.

## Introduction

1  
2  
3  
4 Photonic crystals are structures with periodic low and high refractive indexes.<sup>[1]</sup> Their most  
5 compelling feature is optical diffractions at a wavelength determined by surrounding dielectrics  
6 and the periodicity and orientation of their lattices.<sup>[2]</sup> The constructive interference of light  
7 results in brilliant structural colors.<sup>[3, 4]</sup> Comparing with the classic top-down fabrication  
8 methods,<sup>[5]</sup> the bottom-up approaches involving colloidal self-assembly have been extensively  
9 studied because of the widely accessible building blocks and the ease of assembling them into  
10 diverse secondary structures.<sup>[6]</sup> The combination of low-cost self-assembly with optical  
11 properties of solid particles makes colloidal photonic crystals promising alternatives to  
12 conventional pigments and organic dyes.<sup>[7, 8]</sup> Their structural colors are brighter and much more  
13 stable than organic dyes because the optical diffraction originates from the periodic arrangement  
14 of materials that do not photobleach. In principle, the colors can be tuned by controlling crystal  
15 periodicity and orientation, thereby providing a widely accessible range of colors using a single  
16 material.<sup>[9]</sup> To this end, many methods have been developed to achieve delicate control over  
17 crystal symmetry and periodicity, aiming to generate structural colors to meet the requirements  
18 of practical applications.<sup>[10]</sup>

19  
20  
21  
22  
23  
24  
25  
26  
27  
28  
29  
30  
31  
32 A few prerequisites exist in using photonic crystals as pigments in place of organic dyes.<sup>[7, 11]</sup>  
33 First, their structural colors should be widely tunable while maintaining stability in daily use.  
34 Second, their further advancement to practical applications, particularly in integrated optical  
35 devices and miniature photonic chips, requires easy access to patterned photonic crystals with  
36 highly controllable colors and domains.<sup>[12]</sup> To this end, the self-assembly of colloidal crystal  
37 arrays from nanospheres has been extensively studied, with many methods being developed for  
38 creating colloidal photonic pigments, including capillary-driven colloidal assembly,<sup>[13]</sup> emulsion-  
39 assisted assembly of microbeads,<sup>[9, 14]</sup> and diverse coating methods.<sup>[15]</sup> Besides, a few advanced  
40 printing techniques are also available to pattern photonic crystals into devices,<sup>[16]</sup> such as inkjet  
41 printing<sup>[17]</sup> and three-dimensional (3D) copolymers deposition.<sup>[18]</sup> Most of these photonic  
42 crystals comprise close-packed nanospheres, so that their structural colors are largely determined  
43 by particle size.<sup>[19]</sup> It, therefore, requires precise size control to produce different colors and then  
44 color mixing for generating multiple colors.<sup>[20]</sup> Another disadvantage associated with the highly  
45 symmetric close-packing of either face-centered cubic or less often hexagonal-phase pigments is  
46 the small tunability of the structural colors. This limitation adds challenges to their use in  
47 developing emerging optical materials and devices for advanced applications such as information  
48  
49  
50  
51  
52  
53  
54  
55  
56  
57  
58  
59  
60  
61  
62  
63  
64  
65

1  
2  
3  
4 encryption, anti-counterfeiting, and sensing, where responsive photonic pigments are highly  
5 desirable for displaying hidden information or sensing target molecules.<sup>[3, 21]</sup> In this work, we  
6 report the development of a class of high-quality photonic pigments that can display stable,  
7 bright, and precisely tunable structural colors. These novel photonic pigments, produced by  
8 magnetic assembly of uniform Fe<sub>3</sub>O<sub>4</sub>@SiO<sub>2</sub> nanorods in colloidal dispersion followed by sol-gel  
9 fixation, feature a body-centered tetragonal lattice and a ribbon-like overall shape. The high  
10 anisotropy of the crystal structure combined with the magnetic shape anisotropy of the building  
11 blocks allows the generation of multiple colors by simply changing the direction of the applied  
12 magnetic field. By taking advantage of the unique optical properties of the tetragonal crystals, we  
13 further demonstrate the development of rotation-asymmetric photonic devices that can display  
14 color switching or distinct images in response to mechanical rotation.

15  
16  
17  
18  
19  
20  
21  
22  
23  
24  
25 Uniform magnetic nanorods were prepared by synthesizing FeOOH nanorods (320 nm in length  
26 and 70 nm in width) using a hydrolysis reaction, coating them with a layer of silica of  
27 controllable thickness, and then reducing them to magnetic Fe<sub>3</sub>O<sub>4</sub> phase with shape preservation  
28 by the silica shells.<sup>[22]</sup> The transmission electron microscopy (TEM) images in **Figures s1a** and  
29 **s1b** demonstrate the excellent uniformity of FeOOH and Fe<sub>3</sub>O<sub>4</sub>@SiO<sub>2</sub> nanorods. The digital  
30 pictures in **Figure 1a** depict the assembly of monodisperse nanorods under a permanent magnet  
31 and the precipitation of resulting large crystals driven by magnetic packing force.<sup>[23]</sup> Under the  
32 applied magnetic field, the sparkling crystals exhibit green color. Under dark-field optical  
33 microscope, the ribbon-like crystal exhibits distinct structural colors at two typical orientations  
34 because of the different periodicity along these two crystal directions (**Figure 1b**). The uniform  
35 yellow (top panel in **Figure 1b**) and green colors (bottom panel in **Figure 1b**) from the ribbon  
36 crystal surface and edge suggest the formation of three-dimensional (3D) structures. Besides,  
37 their structural colors can be readily tuned by the magnetic field direction: changing the field  
38 direction from horizontal to vertical leads to a continuous redshift of the perceived colors from  
39 blue to green, yellow, and red (**Figure 1c**).

40  
41  
42  
43  
44  
45  
46  
47  
48  
49  
50  
51  
52 Stable photonic pigments were formed by fixing the assembled colloidal crystals using sol-gel  
53 chemistry, involving the hydrolysis of tetraethoxysilane (TEOS) to produce colloidal silica to  
54 glue the adjacent rods together (**Figure 1a**).<sup>[24]</sup> An additional silica layer is coated on the  
55 assembled crystals in synchrony with the crystal fixation. This sequence of events produces high-  
56 quality photonic pigments that maintain the structural integrity and crystal characteristics even  
57  
58  
59  
60  
61  
62  
63  
64  
65

1  
2  
3  
4 after removing the magnetic field, making it possible to use these anisotropic pigments for  
5 characterization and practical applications. **Figures s1c** and **s1d** show two different projections  
6 of the photonic pigments with centered rectangular and rectangular symmetries, respectively.  
7 **Figure s1c** demonstrates a highly porous superlattice largely due to offset packing of the  
8 nanorods, which, combined with **Figure s1d**, reveals the perfect structural order and crystallinity.  
9 To acquire more crystallographic information of this photonic pigment, we performed electron  
10 tomography and obtained three-dimensional crystal structure through volume rendering of a  
11 series of two-dimensional (2D) TEM projections (**Figure 1d**). The projection in the left panel of  
12 **Figure 1e** produces the same pattern as **Figure s1c**, with the centered rectangular 2D lattice  
13 mapped on the TEM image. Interestingly, this projection evolves to a rectangular 2D lattice  
14 (right panel in **Figure 1e**) when the 3D volume rendering rotates 45°, with the mapped lattice  
15 symmetry being identical to the one in **Figure s1d**. This experimental observation (**Supporting**  
16 **Video 1**) suggests that these two highly related lattices come from colloidal crystal projections of  
17 (110) and (100) facets along  $\langle 110 \rangle$  and  $\langle 100 \rangle$  crystal directions, respectively. Another structural  
18 analysis that could benefit from electron tomography is the direct observation of transverse  
19 crystal symmetry by acquiring a horizontal cross-section of the 3D volume rendering. As shown  
20 in **Figure 1f**, we observe a square 2D lattice in this crystal plane rather than the hexagonal lattice  
21 often observed in colloidal assemblies featuring close packing. This important evidence implies  
22 that magnetic nanorods in the photonic pigments do not favor close packing, despite the hard  
23 contact of their surfaces. The square transverse symmetry also demonstrates the extraordinary  
24 rod packing along the  $\langle 001 \rangle$  crystal directions, which in combination with rod packing in the  
25 other two crystal directions suggests a body-centered tetragonal crystal. The projection schemes  
26 of the three typical facets, as shown in **Figure 1g**, agree well with experimental observations,  
27 confirming the unique tetragonal crystal structures of the photonic pigments.

28  
29  
30  
31  
32  
33  
34  
35  
36  
37  
38  
39  
40  
41  
42  
43  
44  
45  
46  
47  
48 Tuning the structural color is possible by carefully controlling silica thickness and crystal  
49 orientation. For example, using 38-nm silica nanoshells (**Figure s2a**) produces photonic  
50 pigments with primary blue and green colors; the binary colors under the dark-field optical  
51 microscope are attributed to random crystal orientation (left panel in **Figure 2a**). Considering the  
52 different periodicity of (100) and (110) facets, one can distinguish the diffraction planes of the  
53 two colors based on Bragg's law. The diffraction from (110) facets occurs at a shorter  
54 wavelength than that from (100) facets, which are consistent with the blue (middle panel in  
55  
56  
57  
58  
59  
60  
61  
62  
63  
64  
65

1  
2  
3  
4 **Figure 2a)** and green (right panel in **Figure 2a)** colors from (110) and (100) planes, respectively.  
5  
6 Increasing silica thickness to 66 nm (TEM image shown in **Figure s2b)** led to green and red  
7  
8 colors (left panel in **Figure 2b)**. TEM images of the assembled crystals in **Figures s2c** and **s2d**  
9  
10 show similar crystal structures as nanorods with a thinner silica coating. Accordingly, the  
11  
12 diffraction from (110) and (100) planes produce green (middle panel in **Figure 2b)** and red  
13  
14 colors (right panel in **Figure 2b)**. The high quality of the photonic pigments is demonstrated by  
15  
16 the bright colors in **Figure s3** and the perfect crystallinity in the large-scale TEM image in  
17  
18 **Figure s4**. Besides, the two primary colors of photonic pigments with a given silica thickness  
19  
20 reveal the crystal-orientation-dependent structural colors. As demonstrated in **Figure 2c**, a set of  
21  
22 optical microscopy images shows the color changes from green to orange and red when the silica  
23  
24 thickness increases from 38 nm to 66 nm. The simultaneous peak shift in **Figure 2d** from 545  
25  
26 nm to 695 nm indicates a gradually increasing periodicity with silica thickness. Another unique  
27  
28 feature of these photonic pigments is their highly porous and interconnected channels, making  
29  
30 the pigments very susceptible to surrounding dielectric changes. We observe remarkable, rapid,  
31  
32 and reversible color changes (green to red) in a small piece of photonic pigment when the 3D  
33  
34 superstructure wets and dries (**Supporting video 2, Figures 2e** and **s5**). A 150-nm shift in  
35  
36 diffraction was observed due to an increased refractive index from 1 (air) to 1.33 (water) in the  
37  
38 pores (**Figure 2f**).

39  
40 The crystal fixation can be easily scaled up for mass production of high-quality, widely tunable  
41  
42 photonic pigments. A series of digital pictures in **Figure 3a** shows three aqueous dispersions of  
43  
44 photonic pigments made of magnetic nanorods with 38-nm, 50-nm, and 66-nm silica shells. In  
45  
46 the absence of a magnetic field, each sample displayed sparkles of mixed colors of individual  
47  
48 pigments due to their random orientations, with blue and green for 38-nm sample (**Supporting**  
49  
50 **video 3**), blue, green, and yellow for 50-nm sample (**Supporting video 4**), yellow and red for  
51  
52 66-nm sample (**Supporting video 5**). In a fixed magnetic field, each colloidal dispersion showed  
53  
54 monochromatic structural colors due to the uniform alignment of all the pigments. When the  
55  
56 field direction increased from 0° to 15° and 30°, the color changed from purple to blue and green  
57  
58 for the 38-nm sample, blue to green and yellow for the 50-nm sample, and cyan to yellow and  
59  
60 red for the 66-nm sample, respectively. These observations demonstrate the easy tuning of  
61  
62 optical diffraction by magnetic fields and thus the widely accessible structural colors. Gradually  
63  
64 switching the field from 0° to 90° changes the crystal from lateral to longitudinal orientations,  
65

1  
2  
3  
4 leading to increased periodicity and redshift of the observed colors. At 90°, the structure colors in  
5 the three samples disappeared because the large periodicity along the <001> crystallographic  
6 direction shifts the diffraction peak to near-infrared regions (see **Table s1** for summarized  
7 periodicity). A careful measurement reveals a shift from 360 nm to 580 nm (**Figure 3b**) and 500  
8 nm to 680 nm (**Figure 3c**) for 38-nm and 66-nm samples, respectively.  
9

10  
11  
12  
13  
14 These observations underpin the important role of magnetic orientation control in creating  
15 multiple structural colors. We further performed synchrotron-based small-angle X-ray scattering  
16 (SAXS) measurement to characterize the collective alignment of pigments under a magnetic field  
17 (**Figure 4a**).<sup>[25]</sup> The acquired pattern in **Figure 4b** has a centered rectangular symmetry under a  
18 vertical magnetic field. This reciprocal lattice corresponds to the X-ray diffraction of the (110)  
19 facets. Switching the magnetic field from the perpendicular to parallel direction relative to  
20 incident light produces an interesting square lattice (**Figure 4c**) that demonstrates the change of  
21 the diffraction from <110> to <001> crystal directions. One measurable consequence of this  
22 event is the increase in periodicity along the light incidence and the corresponding redshift of  
23 diffraction. A linear profile of the diffraction patterns of (110) facets, obtained under a vertical  
24 magnetic field, is plotted in **Figure 4d**, exhibiting several characteristic peaks in the measured  $q$   
25 range with position ratios ( $q_n/q_1$ , where  $q_n$  refers to the  $n$ th peak) of 1, 2, 3, 4, 6, and 9. Based on  
26 these diffraction peaks, the periodicity between (110) crystal planes is calculated as 144.035 nm  
27 (**Table s1**). **Figure 4e** shows a few representative linear profiles of the SAXS patterns measured  
28 under a horizontal magnetic field. The defined peaks are detectable even in the fifth order, which,  
29 together with the ninth diffraction peak in the vertical configuration, validates the high  
30 uniformity and perfect crystallinity of the photonic pigments. It is worth highlighting that the  
31 efficient orientation control is enabled by the magnetic anisotropy of the Fe<sub>3</sub>O<sub>4</sub> nanorods, making  
32 the long axes of both the constituent nanorods and the photonic pigments parallel to the external  
33 magnetic field.<sup>[26]</sup>  
34  
35  
36  
37  
38  
39  
40  
41  
42  
43  
44  
45  
46  
47  
48  
49

50  
51 By taking advantage of the efficient magnetic alignment of anisotropic pigments, we further  
52 develop rotation-asymmetric photonic devices that can exhibit dynamic color-switching or  
53 display distinct patterns in response to mechanical rotation. This unconventional optical device is  
54 achieved by magnetically aligning the photonic pigments in a photocurable polymer film and  
55 fixing their orientation in different color domains. When a horizontal magnetic field was used  
56 during photopolymerization, the photonic pigments in the polymer matrix exhibited a uniform  
57  
58  
59  
60  
61  
62  
63  
64  
65

1  
2  
3  
4 blue color (**Figure 5a**). Increasing the magnetic field orientation relative to the film surface led  
5 to a color change to green and red due to increased periodicity. For horizontal alignment, the  
6 unidirectional in-plane crystal orientation was also demonstrated by the apparent birefringence in  
7 the photonic film, which has orientation-dependent transmittance under two cross polarizers  
8 (**Figure 5b**). When the pigment orientation was parallel to the polarizer or analyzer (at  $0^\circ$ ), the  
9 film became dark due to the low transmittance of light. At  $45^\circ$ , the film appeared brightest,  
10 indicating the highest transmittance (**Supporting video 6**). These optical effects demonstrate the  
11 good alignment of the photonic pigments to the applied magnetic field. In conventional opal and  
12 inverse opal pigments, their responses to viewing angle changes are symmetric due to the high  
13 crystal symmetry. Our anisotropically structured photonic pigments can break this limitation by  
14 carefully controlling the crystal orientation in the polymer film. **Figure 5c** illustrates the tilted  
15 alignment of the photonic pigments in the solid film and their re-alignment upon rotation.  
16 Because the photonic pigments were magnetically aligned along a pre-designed direction,  
17 clockwise and counterclockwise rotation decreased and increased the angle between the long  
18 axis of the photonic crystals and incident direction of light, leading to opposite blueshift and  
19 redshift of the structural colors, respectively (**Figures 5d** and **5e**). If the film was rotated in the x-  
20 y plane, it exhibited interesting on-off switching of the structural colors. As shown in **Figure 5f**,  
21 this in-plane rotation changed the light incident angle because of the tilted crystal alignment,  
22 making the diffraction peaks shifting out of the visible spectrum. The onset of this principle can  
23 display distinct visual effects depending on initial incident angles. As shown in the left panels  
24 (incident angle= $30^\circ$ ) of **Figure 5g**, the initial green color of a photonic film made by  
25 unidirectional alignment of pigments ( $\sim 30^\circ$  to film surface) disappeared due to the rotation-  
26 induced decrease in incident angle and the ensuing blueshift of the diffraction peak to ultraviolet  
27 (UV). When the incident angle increased to  $40^\circ$ , the film appeared red uniformly, which changed  
28 to blue during the same rotation in the x-y plane (right panel in **Figure 5g**). The concept  
29 underlying this optical transition is the rotation-induced change of the incident angle, which is  
30 enabled by and unique to the anisotropic photonic pigments. To demonstrate potential  
31 applications of this concept, we developed photonic films by patterning the pigments along pre-  
32 designed directions in each domain (represented by blue and green crystals in the right and left  
33 parts of the scheme in **Figure 5h**, respectively) by sequential polymerization of the film under  
34 the presence of a photomask. The photonic pigments in the two domains were aligned  
35  
36  
37  
38  
39  
40  
41  
42  
43  
44  
45  
46  
47  
48  
49  
50  
51  
52  
53  
54  
55  
56  
57  
58  
59  
60  
61  
62  
63  
64  
65



1  
2  
3  
4 symmetrically, with the same tilting angle ( $\sim 30^\circ$ ) to the film surface in opposite tilting directions  
5  
6 (**Figure 5h**). Rotating such a patterned photonic film in the x-y plane led to two distinct visual  
7  
8 effects depending on the incident angle. When the incident angle was  $\sim 40^\circ$ , the top “triangle”  
9  
10 domain appeared blue, while the bottom “square” domain exhibited red because of the tilting-  
11  
12 induced variation in incident angles. Simply rotating the film by  $180^\circ$  in the x-y plane led to  
13  
14 color switching in the two domains due to the changes in their incident geometry (top panels in  
15  
16 **Figure 5i** and **Supporting video 7**). If the incident angle decreased to  $30^\circ$ , the diffraction in the  
17  
18 two domains would blueshift, with red “square” changing to green and blue “triangle”  
19  
20 disappeared due to the shift of its photonic bandgap to the UV region (**Figures s6a and s6b**).  
21  
22 Interestingly, rotating such a film by  $180^\circ$  in the x-y plane changed the shape of the perceived  
23  
24 pattern from a “square” to a “triangle,” which was caused by switching the two domains (bottom  
25  
26 panels in **Figure 5i**). In another design, a photonic film was prepared based on the same concept  
27  
28 to display distinct images. As demonstrated in the left panels of **Figure 5j**, the observed patterns  
29  
30 changed from a 2D matrix of circles to a one-dimensional (1D) linear array upon  $180^\circ$  rotation. If  
31  
32 the incident angle increased to  $40^\circ$  (**Figure s6c**), the two encrypted images could be  
33  
34 simultaneously observed with red and blue colors in each domain, and their colors switch during  
35  
36 rotation (**Supporting video 8**). The programmable optical performance underpins the importance  
37  
38 of orientational control over the current photonic pigments in developing advanced optical  
39  
40 devices.

39  
40 In summary, we have developed photonic pigments by the magnetic assembly of  $\text{Fe}_3\text{O}_4@\text{SiO}_2$   
41  
42 nanorods, which can produce multiple colors in response to the varying magnetic field direction.  
43  
44 The magnetic shape anisotropy of nanorods induces the preferred offset rod packing, producing  
45  
46 tetragonal crystals featuring hard contact, anisotropic non-close-packing, and well-defined and  
47  
48 interconnected channels. Due to their non-close-packing nature, the photonic pigments contain  
49  
50 large pores for accommodating fast and sensitive colorimetric responses to surrounding dielectric  
51  
52 changes. More importantly, the structural and magnetic anisotropy of the photonic pigments  
53  
54 enables precise orientation control using magnetic means so that they can be easily aligned along  
55  
56 pre-designed directions for desirable structural colors and further produce patterned photonic  
57  
58 films. These unique features enable the design and fabrication of rotation-asymmetric photonic  
59  
60 devices that can exhibit dynamic color-switching or display varying patterns and encrypted  
61  
62 information upon rotation. As the materials synthesis is highly scalable and the magnetic  
63  
64  
65

1  
2  
3  
4 assembly is straightforward and robust, our photonic pigments hold great promise for creating  
5 many advanced optical devices, including colorimetric sensors, anti-counterfeiting devices, and  
6 multicolor passive photonic displays.  
7  
8  
9

## 10 11 **Supporting Information**

12  
13  
14 Supporting Information is available from the Wiley Online Library or the author.  
15  
16  
17

## 18 19 **Acknowledgements**

20  
21 The authors are grateful for the financial support from the U.S. National Science Foundation  
22 (CHE-1808788). The electron tomography work done at UCI is supported by the U.S. National  
23 Science Foundation (CHE-1900401). This research used resources of the Center for Functional  
24 Nanomaterials, which is a U.S. DOE Office of Science Facility, at Brookhaven National  
25 Laboratory under Contract No. DE-SC0012704. This research used beamline 7.3.3 of the  
26 Advanced Light Source, which is a DOE Office of Science User Facility under contract no. DE-  
27 AC02-05CH11231. Acknowledgment is also made to the Central Facility for Advanced  
28 Microscopy and Microanalysis at UCR for help with TEM analysis.  
29  
30  
31  
32  
33  
34  
35  
36  
37  
38

39 Received: ((will be filled in by the editorial staff))

40  
41 Revised: ((will be filled in by the editorial staff))

42  
43 Published online: ((will be filled in by the editorial staff))  
44  
45  
46  
47  
48

## 49 **References**

- 50  
51 [1] J. D. Joannopoulos, P. R. Villeneuve, S. Fan, *Nature* 1997, 386, 143; J. H. Moon, S. Yang, *Chem.*  
52 *Rev.* 2010, 110, 547.  
53 [2] Y. Zhao, Z. Xie, H. Gu, C. Zhu, Z. Gu, *Chem. Soc. Rev.* 2012, 41, 3297; Z. Li, Y. Yin, *Adv. Mater.*  
54 2019, 31, 1807061.  
55 [3] J. Ge, Y. Yin, *Angew. Chem. Int. Ed.* 2011, 50, 1492.  
56 [4] H. Li, C. Li, W. Sun, Y. Wang, W. Hua, J. Liu, S. Zhang, Z. Chen, S. Wang, Z. Wu, *Adv. Mater.* 2019,  
57 31, 1900388; R. D. Meade, A. Rappe, K. Brommer, J. Joannopoulos, O. Alerhand, *Phys. Rev. B* 1993, 48,  
58 8434.  
59  
60  
61  
62  
63  
64  
65

- 1  
2  
3  
4 [5] J. Wang, Y. Zhang, S. Wang, Y. Song, L. Jiang, *Acc. Chem. Res.* 2011, 44, 405; S. Takahashi, K.  
5 Suzuki, M. Okano, M. Imada, T. Nakamori, Y. Ota, K. Ishizaki, S. Noda, *Nat. Mater.* 2009, 8, 721; D. Liu, F.  
6 Zhou, C. Li, T. Zhang, H. Zhang, W. Cai, Y. Li, *Angew. Chem. Int. Ed.* 2015, 54, 9596.  
7 [6] Z. Cai, Z. Li, S. Ravaine, M. He, Y. Song, Y. Yin, H. Zheng, J. Teng, A. Zhang, *Chem. Soc. Rev.* 2021;  
8 G. von Freymann, V. Kitaev, B. V. Lotsch, G. A. Ozin, *Chem. Soc. Rev.* 2013, 42, 2528; D. V. Talapin, J.-S.  
9 Lee, M. V. Kovalenko, E. V. Shevchenko, *Chem. Rev.* 2010, 110, 389.  
10 [7] E. S. Goerlitzer, R. N. Klupp Taylor, N. Vogel, *Adv. Mater.* 2018, 30, 1706654.  
11 [8] Y. Wang, H. Cui, Q. Zhao, X. Du, *Matter* 2019, 1, 626.  
12 [9] J. G. Park, S. H. Kim, S. Magkiriadou, T. M. Choi, Y. S. Kim, V. N. Manoharan, *Angew. Chem. Int.*  
13 *Ed.* 2014, 53, 2899.  
14 [10] H. S. Lee, J. H. Kim, J. S. Lee, J. Y. Sim, J. Y. Seo, Y. K. Oh, S. M. Yang, S. H. Kim, *Adv. Mater.* 2014,  
15 26, 5801; F. Fu, L. Shang, Z. Chen, Y. Yu, Y. Zhao, *Sci. Robot.* 2018, 3.  
16 [11] L. Shang, W. Zhang, K. Xu, Y. Zhao, *Materials Horizons* 2019, 6, 945; W. Hong, Z. Yuan, X. Chen,  
17 *Small* 2020, 16, 1907626; R. Vaz, M. F. Frasco, M. G. F. Sales, *Nanoscale Advances* 2020, 2, 5106.  
18 [12] M. Wang, L. He, W. Xu, X. Wang, Y. Yin, *Angew. Chem. Int. Ed.* 2015, 54, 7077.  
19 [13] A. M. Brozell, M. A. Muha, A. N. Parikh, *Langmuir* 2005, 21, 11588; D. Liu, R. Aleisa, Z. Cai, Y. Li, Y.  
20 Yin, *Matter* 2021, 4, 927; J. H. Moon, G. R. Yi, S. M. Yang, D. J. Pine, S. B. Park, *Adv. Mater.* 2004, 16, 605.  
21 [14] S.-H. Kim, J.-G. Park, T. M. Choi, V. N. Manoharan, D. A. Weitz, *Nat. Commun.* 2014, 5, 1; L.  
22 Shang, Y. Cheng, Y. Zhao, *Chem. Rev.* 2017, 117, 7964; Y. Zhao, Y. Cheng, L. Shang, J. Wang, Z. Xie, Z. Gu,  
23 *Small* 2015, 11, 151; M. Xiao, Z. Hu, Z. Wang, Y. Li, A. D. Tormo, N. Le Thomas, B. Wang, N. C. Gianneschi,  
24 M. D. Shawkey, A. Dhinojwala, *Sci. Adv.* 2017, 3, e1701151; T. M. Choi, J.-G. Park, Y.-S. Kim, V. N.  
25 Manoharan, S.-H. Kim, *Chem. Mater.* 2015, 27, 1014.  
26 [15] C. García Núñez, W. T. Navaraj, F. Liu, D. Shakthivel, R. Dahiya, *ACS Appl. Mater. Interfaces* 2018,  
27 10, 3058; D. Xia, A. Biswas, D. Li, S. R. Brueck, *Adv. Mater.* 2004, 16, 1427; H. Yang, P. Jiang, *Langmuir*  
28 2010, 26, 13173.  
29 [16] A. C. Arsenault, D. P. Puzzo, I. Manners, G. A. Ozin, *Nat. Photonics* 2007, 1, 468; J. Hou, M. Li, Y.  
30 Song, *Angew. Chem. Int. Ed.* 2018, 57, 2544.  
31 [17] J. Wang, L. Wang, Y. Song, L. Jiang, *J. Mater. Chem. C* 2013, 1, 6048; R. Shanker, S. Sardar, S.  
32 Chen, S. Gamage, S. Rossi, M. P. Jonsson, *Nano Lett.* 2020, 20, 7243; W. Li, Y. Wang, M. Li, L. P. Garbarini,  
33 F. G. Omenetto, *Adv. Mater.* 2019, 31, 1901036.  
34 [18] B. M. Boyle, T. A. French, R. M. Pearson, B. G. McCarthy, G. M. Miyake, *ACS nano* 2017, 11, 3052;  
35 S. Liu, Y. Yang, L. Zhang, J. Xu, J. Zhu, *J. Mater. Chem. C* 2020, 8, 16633.  
36 [19] Y. Zhao, Z. Xie, H. Gu, L. Jin, X. Zhao, B. Wang, Z. Gu, *NPG Asia Mater.* 2012, 4, e25; Y. Zhao, L.  
37 Shang, Y. Cheng, Z. Gu, *Acc. Chem. Res.* 2014, 47, 3632; R. C. Schroden, M. Al-Daous, C. F. Blanford, A.  
38 Stein, *Chem. Mater.* 2002, 14, 3305.  
39 [20] H. Kim, J. Ge, J. Kim, S.-e. Choi, H. Lee, H. Lee, W. Park, Y. Yin, S. Kwon, *Nature Photon.* 2009, 3,  
40 534.  
41 [21] Z. Li, F. Yang, Y. Yin, *Adv. Funct. Mater.* 2020, 30, 1903467.  
42 [22] Z. Li, J. Jin, F. Yang, N. Song, Y. Yin, *Nat. Commun.* 2020, 11, 1; W. Xu, M. Wang, Z. Li, X. Wang, Y.  
43 Wang, M. Xing, Y. Yin, *Nano Lett.* 2017, 17, 2713; Z. Li, M. Wang, X. Zhang, D. Wang, W. Xu, Y. Yin, *Nano*  
44 *Lett.* 2019, 19, 6673.  
45 [23] L. He, M. Wang, J. Ge, Y. Yin, *Acc. Chem. Res.* 2012, 45, 1431; Z. Li, C. Qian, W. Xu, C. Zhu, Y. Yin,  
46 *Sci. Adv.* 2021, 7, eabh1289.  
47 [24] Y. Hu, L. He, Y. Yin, *Angewandte Chemie* 2011, 123, 3831.  
48 [25] K. Deng, X. Huang, Y. Liu, L. Xu, R. Li, J. Tang, Q.-l. Lei, R. Ni, C. Li, Y. S. Zhao, *Nano Lett.* 2020, 20,  
49 7367.  
50 [26] M. Wang, C. Gao, L. He, Q. Lu, J. Zhang, C. Tang, S. Zorba, Y. Yin, *J. Am. Chem. Soc.* 2013, 135,  
51 15302.  
52  
53  
54  
55  
56  
57  
58  
59  
60  
61  
62  
63  
64  
65

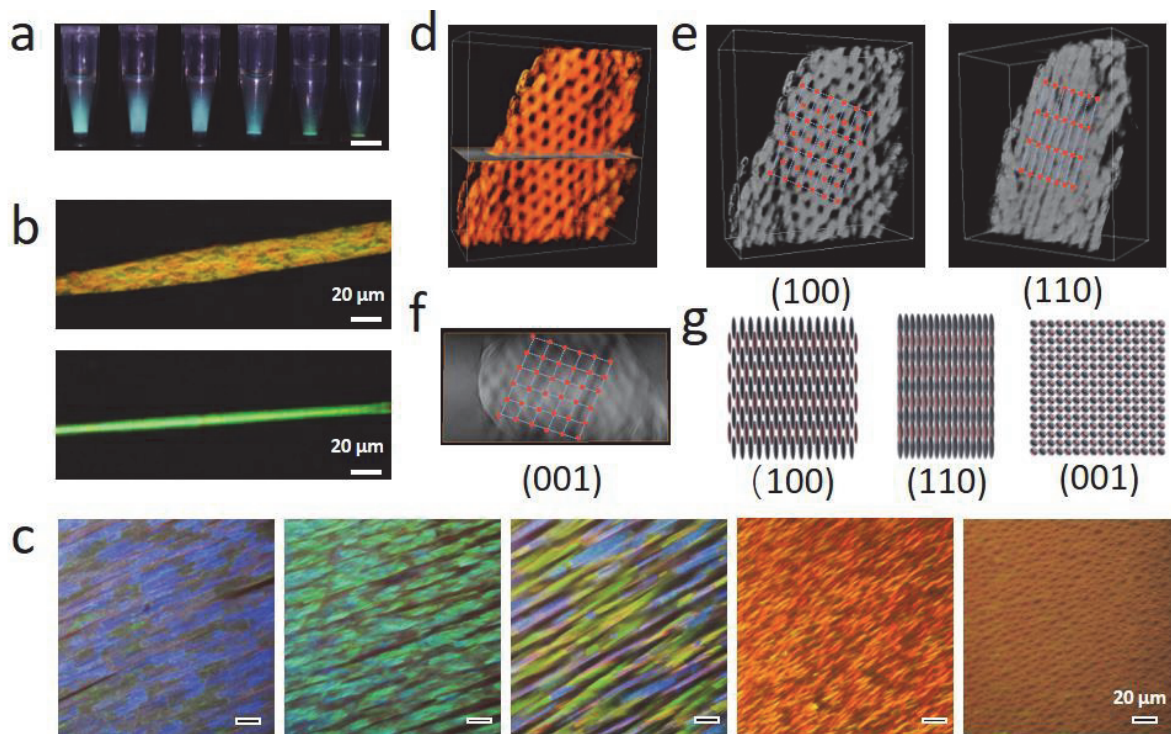


**Figure 1.** (a) Digital pictures showing the self-assembly of  $\text{Fe}_3\text{O}_4@\text{SiO}_2$  nanorods in the mixture of water and ethanol under a vertical magnetic field. Scale bar: 2 mm. (b) Dark-field optical microscopy images of the assembled photonic crystals with exposed (100) and (110) facets shown in the top and bottom panels, respectively. (c) Dark-field optical microscopy images of the self-assembled photonic crystal in magnetic fields with varying directions from horizontal (left) to vertical (right). (d) 3D rendering of TEM tomography of a photonic crystal. (e) 3D rendering of the same crystal with two different exposed facets as indicated, leading to two typical projection patterns. (f) A horizontal cross-section of the reconstructed photonic crystal with exposed (001) facets, which reveals the rod packing along  $\langle 001 \rangle$  crystal direction. (g) Schematic illustrations of the projections of the photonic crystal with exposed (100), (110), and (001) facets, demonstrating the rod packing along the  $\langle 100 \rangle$ ,  $\langle 110 \rangle$ , and  $\langle 001 \rangle$  crystal directions, respectively.

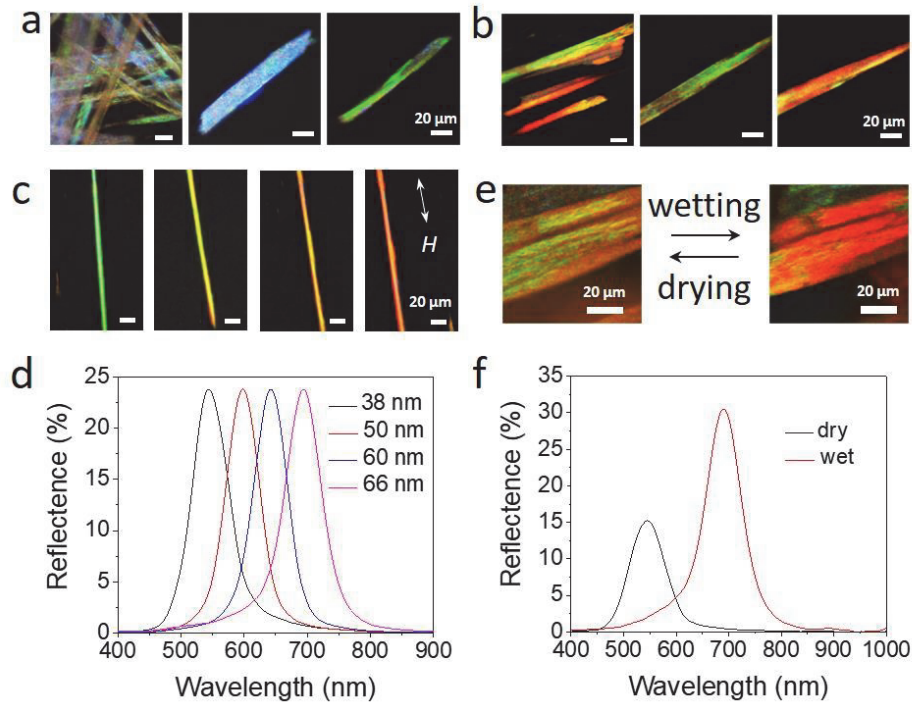


**Figure 2.** (a, b) Dark-field optical microscopy images of the photonic pigments produced by magnetic assembly of  $\text{Fe}_3\text{O}_4@\text{SiO}_2$  nanorods with the silica shell thickness of 38 nm (a) and 66 nm (b). The three images in (a) and (b) exhibit the photonic pigments with random orientations (left) and alignment along  $\langle 110 \rangle$  (middle) and  $\langle 100 \rangle$  (right) directions (relative to the image plane). (c) Dark-field optical microscopy images of the photonic crystals with the silica thickness gradually increasing from 38 nm to 50 nm, 60 nm, and 66 nm from left to right. The white arrow indicates the magnetic field direction. (d) The corresponding reflection spectra of the assembled crystals from nanorods with different silica thicknesses. (e, f) Dark-field optical microscopy images (e) and the reflection spectra (f) of a crystal upon wetting by water and drying in air.

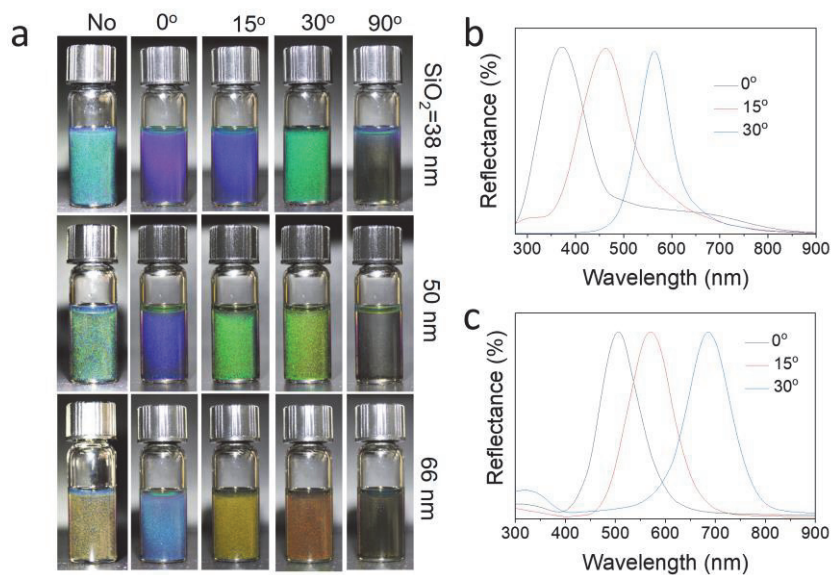


**Figure 3.** (a) Digital pictures of the dispersions of photonic pigments under magnetic fields of varying directions. (b, c) The reflection spectra of crystals aligned under magnetic fields of different directions. The silica shell thickness is 38 nm in (b) and 66 nm in (c).

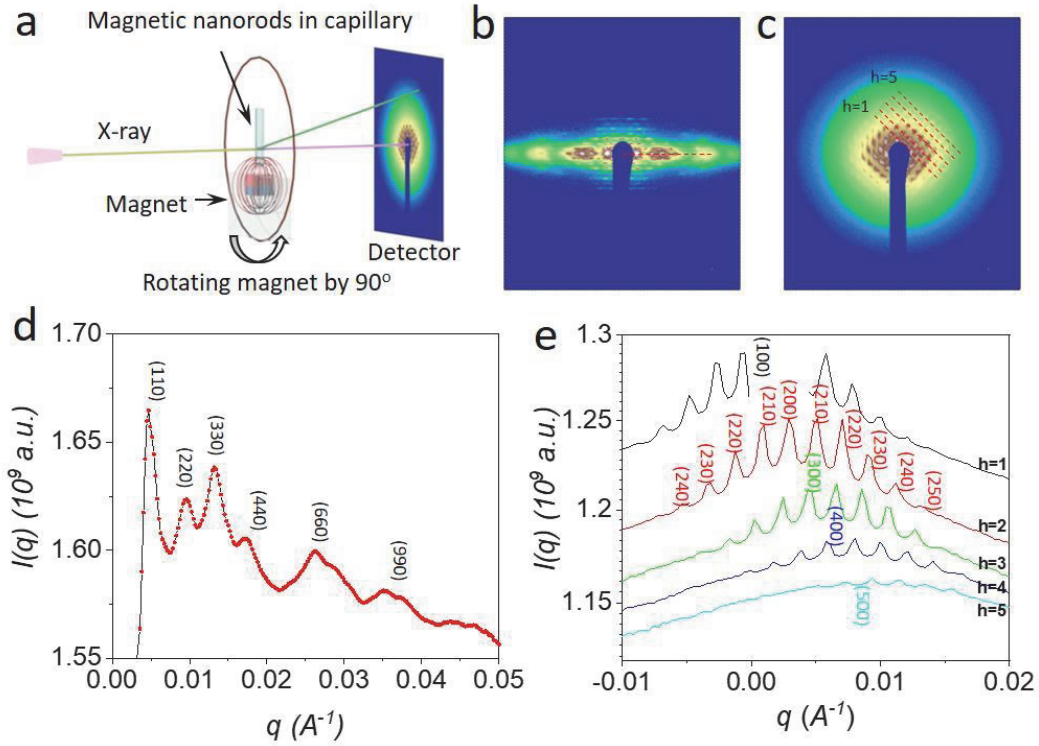


**Figure 4.** SAXS measurement of the photonic crystals. **(a)** Schematic illustration of the setup. **(b), c)** SAXS patterns of the crystals under a vertical **(b)** and horizontal **(c)** magnetic field. **(d, e)** Linear profile of the scattering patterns under a vertical **(d)** and horizontal **(e)** magnetic field.

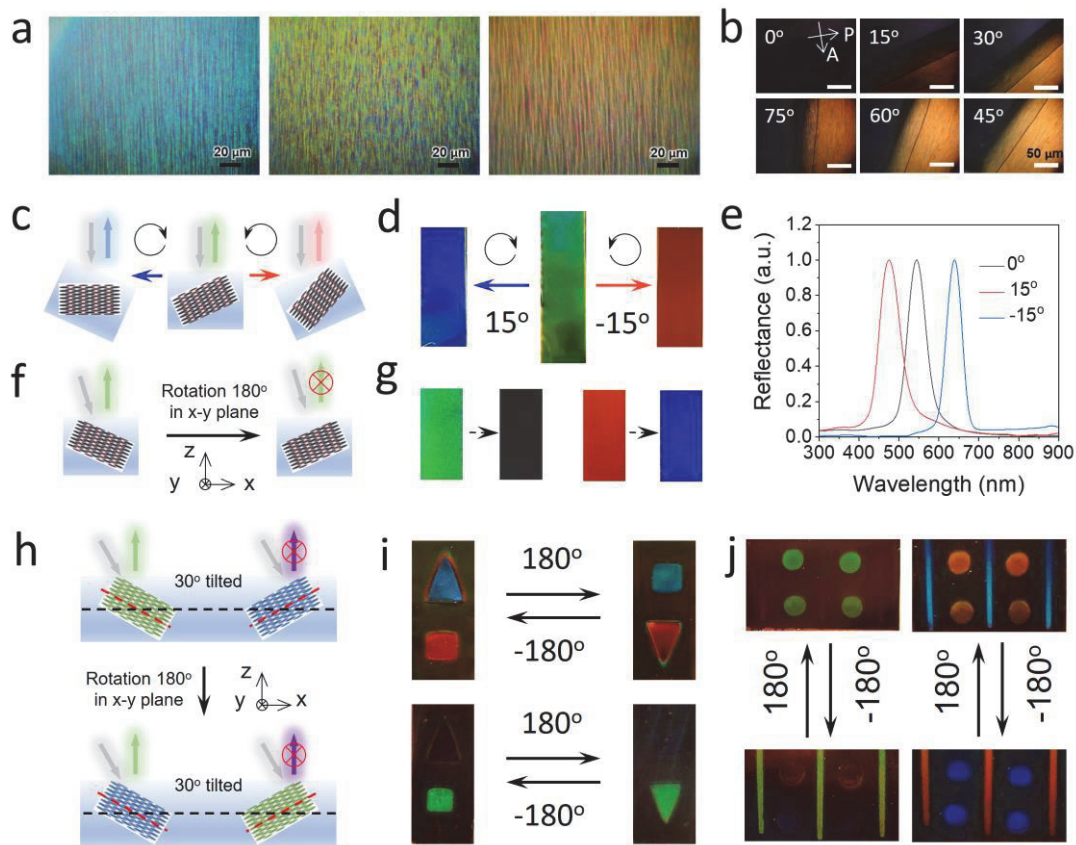


**Figure 5.** Highly tunable multicolor photonic pigments for rotation-asymmetric mechanochromic photonic devices. **(a)** Dark-field microscopy images of the photonic pigments aligned along different directions in photonic films. **(b)** Polarized microscopy images of the photonic films under different rotation angles. The directions of the polarizer (P) and analyzer (A) are shown in white arrows. The angle between the rod alignment and the polarizer direction is also labeled in each image. **(c)** Schematic illustration of the rotation-asymmetric photonic film by magnetically aligning the photonic pigments along a pre-designed direction. **(d)** Digital photos showing the color changes of the photonic film in response to clockwise and counterclockwise rotation. **(e)** The corresponding reflection spectra of the film during the opposite rotation. **(f)** Schematic illustration of changes in the incident angle and structural colors of the photonic film during rotation by  $180^\circ$  in the x-y plane. **(g)** Digital photos of photonic films before and after rotation. The photonic pigments are aligned along  $30^\circ$  to the film surface. The incident angle in the left and right panels is  $30^\circ$  and  $40^\circ$ , respectively. **(h)** Schematic illustration of the alignment of the photonic pigments in the solid film for emerging mechanochromic responses. **(i-j)** Digital photos of two photonic films showing the displayed patterns and their color changes in response



1  
2  
3  
4 to mechanical rotation. The incident angle is  $40^\circ$  in the top panel of **(i)** and right panel of **(j)**,  
5  
6 while it is  $30^\circ$  in the other two panels. The positive and negative angles represent clockwise and  
7  
8 counterclockwise mechanical rotation, respectively.  
9  
10  
11  
12  
13  
14  
15  
16  
17  
18  
19  
20  
21  
22  
23  
24  
25  
26  
27  
28  
29  
30  
31  
32  
33  
34  
35  
36  
37  
38  
39  
40  
41  
42  
43  
44  
45  
46  
47  
48  
49  
50  
51  
52  
53  
54  
55  
56  
57  
58  
59  
60  
61  
62  
63  
64  
65

1  
2  
3  
4 **Table of Contents**  
5  
6

7 A novel multicolor photonic pigment is developed by the magnetic assembly of  $\text{Fe}_3\text{O}_4$  nanorods  
8 into tetragonal photonic crystals. Its dynamic color tuning and precise orientational control  
9 enable convenient printing of structural colored patterns and designing rotation-asymmetric  
10 photonic devices.  
11  
12  
13

